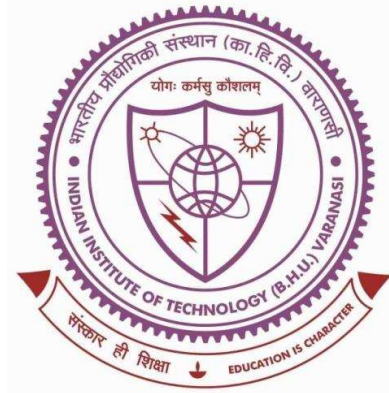


Mechanical and Corrosion Behaviour of Maraging Steel Processed by Powder Bed Fusion using Laser Beam



Thesis submitted in partial fulfilment for the
award of degree

Doctor of Philosophy

By

Jaydeep Vishwakarma

DEPARTMENT OF METALLURGICAL ENGINEERING
INDIAN INSTITUTE OF TECHNOLOGY
(BANARAS HINDU UNIVERSITY)
VARANASI-221005

17141004

2023

CERTIFICATE

It is certified that the work contained in the thesis titled "*Mechanical and Corrosion behaviour of Maraging Steel processed by Powder Bed Fusion using Laser Beam*" by "*Jaydeep Vishwakarma*" has been carried out under my supervision and this work has not been submitted elsewhere for a degree.

It is further certified that the student has fulfilled all the requirements of Comprehensive, Candidacy and SOTA for the award of PhD degree.

NC Santhi Srinivas
Prof. N.C. Santhi Srinivas

(Supervisor)

Department of Metallurgical Engineering
Indian Institute of Technology
(Banaras Hindu University)
Varanasi- 221005


Dr. Kausik Chattopadhyay

(Co-supervisor)

Department of Metallurgical Engineering
Indian Institute of Technology
(Banaras Hindu University)
Varanasi- 221005

DECLARATION BY THE CANDIDATE

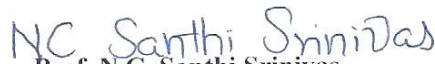
I, "*Jaydeep Vishwakarma*", certify that the work embodied in this thesis is my own bona fide work and carried out by me under the supervision of "*Prof. N. C. Santhi Srinivas*" and "*Dr. Kausik Chattopadhyay*" from "*July 2017*" to "*December 2022*", at the "*Department of Metallurgical Engineering*", Indian Institute of Technology (BHU), Varanasi. The matter embodied in this thesis has not been submitted for the award of any other degree/diploma. I declare that I have faithfully acknowledged and given credits to the research workers wherever their works have been cited in my work in this thesis. I further declare that I have not wilfully copied any other's work, paragraphs, text, data, results, *etc.*, reported in journals, books, magazines, reports dissertations, theses, *etc.*, or available at websites and have not included them in this thesis and have not cited as my own work.

Date *22/05/2023*


Jaydeep Vishwakarma

CERTIFICATE BY THE SUPERVISORS

It is certified that the above statement made by the student is correct to the best of our knowledge.


Prof. N.C. Santhi Srinivas
(Supervisor)

Department of Metallurgical Engineering
Indian Institute of Technology
(Banaras Hindu University)
Varanasi- 221005


Dr. Kausik Chattopadhyay
(Co-supervisor)

Department of Metallurgical Engineering
Indian Institute of Technology
(Banaras Hindu University)
Varanasi- 221005

Prof. Sunil Mohan


(Head of the Department)

Department of Metallurgical Engineering
Indian Institute of Technology (Banaras Hindu University)

COPY RIGHT TRANSFER CERTIFICATE

Title of the Thesis:

“Mechanical and Corrosion behaviour of Maraging Steel processed by Powder Bed Fusion using Laser Beam”

Name of the Student: Jaydeep Vishwakarma

COPYRIGHT TRANSFER

The undersigned hereby assigns to the Indian Institute of Technology (Banaras Hindu University) Varanasi all rights under copyright that may exist in and for the above thesis submitted for the award of the "**Doctor of Philosophy**".

Date: 22/05/2023

Place: Varanasi



Jaydeep Vishwakarma

Note: However, the author may reproduce or authorize others to reproduce material extracted verbatim from the thesis or derivative of the thesis for author's personal use provided that the source and the Institute's copyright notice are indicated.

Dedicated

To

My Beloved Parents

and

My Elder and Younger

Brother

ACKNOWLEDGEMENTS

I am very grateful and indebted to my supervisor Professor N.C. Santhi Srinivas, Department of Metallurgical Engineering, for her consistent help, encouragement and valuable discussions during the entire period of my research work. The way she teaches me is really excellent and she is always a source of inspiration for me. Madam always supported me in both research and in personal problems. I would not have been able to complete the thesis without her utmost involvement and invaluable efforts.

Besides my Supervisor, I would also like to thank my Co-supervisor Dr. K. Chattopadhyay, Department of Metallurgical Engineering for their help and support during my research work.

I would also like to thank members of RPEC: Dr. Meghanshu Vashista, Department of Mechanical Engineering, and Dr. R. Manna, Department of Metallurgical Engineering for their insightful comments and encouragement. I am also thankful to Prof. Vakil Singh for their valuable guidance in carrying out in-depth analysis of the outcomes of the research work.

I sincerely thank Prof. Sunil Mohan, Head, Department of Metallurgical Engineering and Prof. N.K. Mukhopadhyay, former Head, Department of Metallurgical Engineering for providing all the research facilities to successfully accomplish my research in the Department. I have a deep sense of gratitude to Dr. Praveen Sathiyamoorthi, Dr. G.S. Mahobia, Dr. A.K. Mondal and all other faculty members of the Department of Metallurgical Engineering, IIT (BHU), for their cooperation and inspiration.

I am also thankful to M/s. Renishaw Metrology Pune, for providing Additive Manufacturing facility and M/s. Bharat Aerospace Metals, Mumbai for providing conventional materials.

I am obliged to all my seniors, especially Dr. G. Sudhakar Rao, Dr. R.S. Rajpurohit, Dr. Vaibhav Pandey, Dr. Preeti Verma, Dr. Ch. Visweswara Rao, Dr. Purna Mishra, Dr. Chandrasekhar, Dr. Pramod, for their constant support in experimental work, making joyful and memorable life and being with my moments of happiness and troubles at IIT (BHU), Varanasi. I am thankful to wonderful juniors and friends Sandeep, Dr. Shravan, Dr. Mudila Dhanunjaya Rao, Amit Yadav, Vineet, Nitesh, Manik, Roopchand, Sarika, Ankit, Vasu Shreyasi, Ishu, Ishwari, and others for their assistance and support. I am also thankful to all my junior students of M. Tech and Ph.D of our group from 2017 to 2022 for their constant support during experimental work.

I am thankful to all the Lab and workshop staff specially Mr. Sushil Ji, Mr. Kamlesh Ji, Mr. Minz Ji, Mr Balwant Ji for making fatigue and tensile specimens, Mr. Anjani Ji, Mr. Balvanth Ji, Mr. Raj Naranyan Ji, Mr. Patel Ji and all lab and office. Last, but not the least, I would like to express my deepest gratitude to my parents Sri. Dhaniram Vishwakarma and Smt. Shavitri Devi, my elder brother Mr. Pradeep Vishwakarma, my younger brother Mr. Prashant Vishwakarma and my sister Ms. Pinkee Vishwakarma for their unconditional support and encouragement to pursue my interest

I also wish to thank all my friends and the persons whose names have not been mentioned on this piece of paper for extending their cooperation directly or indirectly.

JAYDEEP VISHWAKARMA

TABLE OF CONTENTS

	Page No.
List of Figures	xiii
List of Tables	xxi
List of Symbols	xxiii
Preface	xxv
CHAPTER 1	
INTRODUCTION AND LITERATURE	1 – 48
1.1 INTRODUCTION	1
1.2 ADDITIVE MANUFACTURING OVER SUBTRACTIVE MANUFACTURING	1
1.3 CLASSIFICATION OF ADDITIVE MANUFACTURING TECHNOLOGIES	2
1.3.1 Powder bed Fusion (PBF)	2
1.3.2 Direct energy deposition (DED)	4
1.3.3 Material Extrusion (ME)	4
1.3.4 Sheet lamination (SL)	5
1.3.5 Binder jetting (BJ)	6
1.3.6 Vat Photopolymerization (VP)	6
1.3.7 Material Jetting (MJ)	7
1.4 Important Factors in PBF/SLM	7
1.4.1 Process Parameters	7
1.4.2 Defects in Powder bed fusion	9
1.4.3 Materials for PBF-LB/SLM	10
1.4.4 Recent developments	11
1.4.5 Powder specifications for SLM	12
1.5 NEED FOR PROCESSING OF STEELS BY ADDITIVE MANUFACTURING	13
1.6 IMPORTANCE OF MARAGING STEEL IN AM	14
1.7 MARAGING STEELS	15
1.7.1 Effect of alloying elements	17
1.7.2 Precipitation behavior of maraging steel	19
1.7.3 Austenite reversion in maraging steel	21
1.8 APPLICATIONS OF ADDITIVE MANUFACTURED MARAGING STEELS	22
1.9 RESEARCH INVESTIGATIONS ON AM MARAGING STEELS	23
1.9.1 TENSILE BEHAVIOUR	23
1.9.2 LOW CYCLE FATIGUE (LCF) BEHAVIOR	30
1.9.3 WEAR BEHAVIOUR	32
1.9.4 EROSION BEHAVIOUR	37
1.9.5 CORROSION BEHAVIOUR	39
1.10 SCOPE OF THE PRESENT WORK	44
1.11 MOTIVATION FOR THE PRESENT WORK	45
1.12 OBJECTIVES OF THE PRESENT INVESTIGATION	48

CHAPTER 2

	MATERIALS AND METHODS	49-62
2.1	INTRODUCTION	49
2.2	MATERIALS	49
2.3	PROCESSING OF POWDERS	50
2.3.1	Powder Bed Fusion using Laser Beam (PBF-LB)	50
2.4	INITIAL CHARACTERIZATION	52
2.4.1	Surface Roughness and Relative density	52
2.4.2	Heat Treatment and Microstructural characterization	52
2.5	MECHANICAL BEHAVIOUR	55
2.5.1	Hardness and Tensile behaviour	55
2.5.2	Fatigue behaviour	56
2.6	TRIBOLOGICAL BEHAVIOUR	57
2.6.1	Wear behaviour	57
2.6.2	Solid Particle Erosion behaviour	59
2.7	CORROSION BEHAVIOUR	60
2.8	CHAPTER SUMMARY	62

CHAPTER 3

	CHARACTERIZATION	63-78
3.1	INTRODUCTION	63
3.2	POWDER CHARACTERIZATION	63
3.2.1	Powder Morphology	63
3.2.2	Density and surface roughness	64
3.3	MICROSTRUCTURAL CHARACTERIZATION	65
3.3.1	Microstructure of as-built (AM) and conventionally manufactured (CM) samples	65
3.3.2	Microstructure of heat-treated AB and CM samples	70
3.4	DISCUSSION	74
3.4.1	Characterization of Powder	74
3.4.2	Relative density and surface roughness	74
3.4.3	Microstructural Characterization	75
3.5	CHAPTER SUMMARY	78

CHAPTER 4

	TENSILE AND LOW CYCLE FATIGUE BEHAVIOUR	79-102
4.1	INTRODUCTION	79
4.2	Influence of Build Orientation on Tensile Behaviour	79
4.2.1	Residual stresses	79
4.2.2	Hardness	80
4.2.3	Tensile behaviour	81
4.3	Influence of Build Orientation on Low Cycle Fatigue Behavior	85
4.3.1	Cyclic Stress Response	86
4.3.2	Fatigue life	88
4.3.3	Cyclic Hysteresis loops	90
4.3.4	Fracture behaviour of LCF tested samples	91
4.4	DISCUSSION	94

4.4.1	Residual stress	94
4.4.2	Hardness	96
4.4.3	Tensile behaviour	96
4.4.4	Low Cycle Fatigue Behaviour	98
4.5	CHAPTER SUMMARY	100

CHAPTER 5

	WEAR AND EROSION BEHAVIOUR	103-124
5.1	INTRODUCTION	103
5.2	Wear and Erosion Behaviour	103
5.2.1	Microstructural Characterization	103
5.2.2	Wear rate	107
5.2.3	Coefficient of friction (COF)	109
5.2.4	Erosion Rate	111
5.2.5	Morphology of worn surfaces	111
5.2.6	Morphology of Eroded Surfaces	114
5.3	Discussion	
5.3.1	Microstructure	117
5.3.2	Wear Behaviour	118
5.3.3	Erosion Behaviour	120
5.3.4	Wear and Erosion Surface Morphology	120
5.4	Wear and Erosion Mechanism	121
5.5	CHAPTER SUMMARY	123

CHAPTER 6

	CORROSION BEHAVIOUR	125-154
6.1	INTRODUCTION	125
6.2	Corrosion Behaviour	125
6.2.1	Microstructural Characterization	125
6.2.2	Open-circuit Potential and Potentiodynamic Polarization	128
6.2.2.1	In As-Built (AB/AR) Condition	128
6.2.2.2	In Heat Treated (HT) Condition	129
6.2.3	Electrochemical Impedance Spectroscopy (EIS)	130
6.2.4	Chemical composition of corroded surfaces	135
6.2.4.1	XPS analysis	135
6.2.4.2	SEM-EDS analysis	141
6.2.5	Corrosion Mechanism	146
6.3	DISCUSSION	150
6.3.1	Microstructural Characterization and Phase analysis	150
6.3.2	Corrosion Behaviour of AB and as received Conventionally Manufactured (CM) specimens	150
6.3.3	Corrosion Behaviour of AM-HT and CM-HT specimens	151
6.3.4	Chemical composition and surface morphology of corroded specimens	152
6.4	CHAPTER SUMMARY	154

CHAPTER 7

	MAJOR CONCLUSIONS AND SUGGESTIONS FOR FUTURE WORK	155-160
7.1	INTRODUCTION	155
7.2	MAJOR CONCLUSION	155
	7.2.1 Initial Characterization	155
	7.2.2 Tensile and Low Cycle Fatigue Behaviour	156
	7.2.3 Wear and Erosion Behaviour	158
	7.2.4 Corrosion Behaviour	159
7.3	SUGGESTIONS FOR FUTURE WORK	160
	REFERENCES	161-175
	PUBLICATIONS AND CONFERENCES	177

LIST OF FIGURES

Figure No.	Figure Caption	Page No.
Fig. 1.1	Process comparison of additive manufacturing and subtractive manufacturing	2
Fig. 1.2	Schematic diagram for Powder bed fusion PBF/SLM	3
Fig. 1.3	Schematic diagram for Direct Energy Deposition (DED)	4
Fig. 1.4	Schematic diagram for Material Extrusion (ME)	5
Fig. 1.5	Schematic diagram for Sheet Lamination (SL)	5
Fig. 1.6	Schematic diagram for Binder Jetting	6
Fig. 1.7	Schematic diagram for Vat Photopolymerization	7
Fig. 1.8	Schematic diagram for Material Jetting	7
Fig. 1.9	(a) Iron-nickel phase diagram (b) Metastable martensite phase transformation	17
Fig. 1.10	As fabricated microstructure (a) top face showing 67° inter layer rotations, (b, c) magnified view of 'a' showing fine and coarse cellular grains, (d) melt pool in transverse face and (e, f) magnified view showing mainly columnar grains.	24
Fig. 1.11	Residual stresses in samples after: (a) as-fabrication (b) heat treatment.	24
Fig. 1.12	(a) Stress-strain response of horizontal (XY-built) and vertical samples (Z-built), (b, c) fractographs of horizontal samples and (d, e) fractographs of vertical samples, both showing ductile fracture	27
Fig. 1.13	(a) Schematic view of high-power laser processing, showing spatter and vaporization (b) increase in spatter with laser power	28
Fig. 1.14	(a) process parameter optimization widow for better part density (b) Stress-strain curves of horizontal and vertical samples in as-built and solution/ aging treated (STAed) conditions.	29
Fig. 1.15	(a) Variation of friction coefficient with time (b) 3D wear track morphology and (c) sectional line profiles of wear track of SLM specimens	33

Fig. 1.16	The friction coefficients (a) and wear losses (b) in the tribological tests of as fabricated sample and nitrided samples. The inserted image shows the depth profiles of wear tracks	34
Fig. 1.17	Worn surfaces of the (a) as-fabricated and (b) aged SLM maraging steel (490 °C for 3 h) and (c, d) the corresponding EDX analysis. The atomic fraction of each element	35
Fig. 1.18	Schematic diagram of the cross-section of wear tracks of (a) SD (b) BD for inferring the bead direction and crack propagation in the specimen and (c) comparison of wear rates after the wear testing with a total wear distance of 90 m under various wear loads and speeds	36
Fig. 1.19	Effect of build direction, heat treatment and sliding orientation on the wear resistance of LPBF maraging steel	37
Fig. 1.20	Variations of erosion rate with: (a) impingement angle and (b) laser scanning speed	38
Fig. 1.21	Potentiodynamic polarization curve	40
Fig.1.22	Corrosion morphology of SLM-processed M300 samples and HIPed samples (a) STA (b) HIP-STA conditions and (c) stress vs strain plots for SLM-processed M300 maraging steel	41
Fig. 1.23	Potentiodynamic polarization curves of the asbuilt, heat-treated, and drag finishing samples	42
Fig. 1.24	(a) Additive manufactured 3D model of a sphere: (b) Tensile loading (c) Fatigue loading (d) surfaces for wear and erosion and (d) surfaces for corrosion, with respect to layer orientation.	46
Fig. 1.25	Schematic presentation of samples built in 0°, 45°, and 90° orientations to the base plate.	47
Fig. 2.1	(a) 3D models of plates and rods with support structure, (b) Schematic view and Renishaw AM250 PBF-LB system and (c) Processed plates and rods with support structure and base plate in different orientations.	51
Fig. 2.2	Heat Treatment (HT) adopted for the present M300 maraging steel	53
Fig. 2.3	(a) 100kN Universal Testing Machine (b) Subsize polished flat tensile samples built in orientation of 0°, 45°, 90° and CM sample (c) Dimensions of subsize tensile sample.	55

Fig. 2.4	(a) 100kN fatigue testing system (b) Polished fatigue sample (c) Geometry of fatigue sample (d) Triangular, fully reversed waveform for axial loading.	57
Fig. 2.5	(a) Pin on Disc (PoD) tribometer setup and (b) samples in different conditions.	58
Fig. 2.6	(a) DUCOM air jet erosion system (b) Eroded samples in different conditions (c) Morphology of erodent particles.	60
Fig. 2.7	(a) Electrochemical experimental setup (b) Polished AB samples in different orientations along with the conventional samples used for corrosion testing.	60
Fig. 3.1	(a) Morphology of M300 Powder particles and (b) Histogram showing powder size distribution.	63
Fig. 3.2	(a) Gas atomized single powder particle showing dendrites and (b) EDS analysis of powder.	64
Fig. 3.3	Optical Micrographs of AM samples of M300 in (a) 0° orientation (b) 45° Orientation and (c) 90° orientations, showing hatch pattern and 67° inter layer rotation in top view and melt pool characteristics in transverse views. Blue colour line shows deposition layers, red circles show voids/pores. Also, N, N+1, N+2 successive deposited layers are shown by yellow arrows.	66
Fig. 3.4	Optical Micrographs of M300 steel: (a) Transverse section of AM sample in 0° orientation showing columnar and cellular grains. Also marked as 1 and 2 (b) CM sample showing coarse equiaxed grains	67
Fig. 3.5	SEM micrographs of transverse section of AM sample in 0° orientation showing: (a) melt pools and (b) magnified view of (a) showing columnar grains (marked as 1) and cellular grains (marked as 2).	68
Fig. 3.6	X-Ray diffraction pattern of powder (M300) and AM samples built in different orientations revealing martensite (<i>bcc</i>) and a small fraction of austenite (<i>fcc</i>).	69
Fig. 3.7	TEM bright field micrographs of 0° AM sample of M300 showing: (a) columnar grains (b) cellular grains and (c) corresponding SAD pattern.	70
Fig. 3.8	Dark field micrograph of 45° AM sample of M300 showing triggered precipitation (as shown by arrows) due to intrinsic heat treatment.	70

Fig. 3.9	Optical micrographs of heat-treated samples of M300 showing lath martensite in (a) transverse section of 0° AM-HT sample and (b) CM-HT sample.	71
Fig. 3.10	X-Ray Diffraction patterns of CM-HT and AM-HT samples built in different orientations revealing martensite (<i>bcc</i>) and reverted austenite (<i>fcc</i>).	72
Fig. 3.11	Microstructure of M300 in 0°AM-HT condition: (a) TEM Bright field micrograph showing reverted austenite and (b) SAD pattern revealing austenite (<i>fcc</i> phase, $a=2.07 \text{ \AA}$), beam direction (B), $z: [-114]$	73
Fig. 3.12	Microstructure of M300 in 45°AM-HT condition:(a) TEM Bright field micrograph showing Ni ₃ Ti precipitates and (b) SAD pattern revealing Ni ₃ Ti (<i>hcp</i> phase, $a=2.02 \text{ \AA}$ $c=8.29 \text{ \AA}$), beam direction (B) $z: [0001]$	73
Fig. 3.13	Microstructure of M300 in 45°AM-HT condition: (a) TEM Bright field micrograph showing Fe ₂ Mo precipitates (b) SAD pattern revealing Fe ₂ Mo (<i>hcp</i> phase, $a=4.75 \text{ \AA}$ and $c=7.76 \text{ \AA}$), beam direction (B) $z: [1-21-3]$	74
Fig. 4.1	Variation of microhardness in different conditions of CM and AM samples.	80
Fig. 4.2	Engineering stress-strain curves of AB samples of M300 steel in different orientations.	81
Fig. 4.3	Engineering stress-strain curves of AM-HT samples of M300 steel in different orientations.	82
Fig. 4.4	Engineering stress-strain curves of as-received and heat-treated CM samples of M300 steel.	82
Fig. 4.5	Fractographs of tensile tested specimens in different conditions (a) 0° AB (b) 45° AB (c) 90° AB (d) 0° HT (e) 45° HT and (f) 90° HT.	84
Fig. 4.6	(a) Cylindrical specimens printed via powder bed fusion in 0°, 45°, and 90° build orientation, (b) Machined and polished fatigue samples (c) LCF testing system with extensometer and (d) Fatigue fractured samples.	85
Fig. 4.7	Schematic diagram depicting the orientation of layers and the alignment of defects with respect to loading axis in samples built in: (a) 0° (b) 45° and (c) 90° orientations.	86

Fig. 4.8	Cyclic stress response of samples at $\pm 0.5\%$ strain amplitude before and after heat treatment: (a) 0° AB, 45° AB, 90° AB and CM samples (b) 0° HT, 45° HT, 90° HT and CM-HT samples.	87
Fig. 4.9	Plots ($ \sigma_c/\sigma_t \times 100$), with the number of cycles and determination of the number of cycles for crack initiation (N_i).	89
Fig. 4.10	Cyclic stress-strain response of samples before and after heat treatment at $0.5N_f$ cycle and $\pm 0.5\%$ strain amplitude: (a) Hysteresis loops of 0° AB, 45° HT, 90° HT and CM samples and (b) Hysteresis loops of 0° HT, 45° HT, 90° HT and CM-HT samples.	90
Fig. 4.11	Fractographs of fatigue tested samples: (a-c) 0° AB and (d-f) 45° AB.	91
Fig. 4.12	Fractographs of fatigue tested samples: (a-c) 90° AB and (d-f) CM sample.	92
Fig. 4.13	Fractographs of fatigue tested samples: (a-c) 0° HT and (d-f) 45° HT.	93
Fig. 4.14	Fractographs of fatigue tested samples: (a-c) 90° HT and (d-f) CM-HT.	94
Fig. 5.1	Schematic presentation of 0° , 45° and 90° built samples used for: (a) wear test sample, 0° AB _w , 45° AB _w and 90° AB _w are mating surfaces with rotating disc and (b) erosion test samples, 0° AB _w , 45° AB _w and 90° AB _w are exposed surfaces in erosion.	104
Fig. 5.2	Microstructure of the as built samples in 0° , 45° , 90° orientation and conventional samples taken from the faces of wear and erosion testing: (a) 0° AB _w (b) 45° AB _w (c) 90° AB _w and (d) CM _w (a') 0° AB _E (b') 45° AB _E (c') 90° AB _E and (d') CM _E .	104
Fig. 5.3	Optical micrographs of 0° as-built samples at higher magnification (a) laser scanning side (b) layers or melt pool side (c) micrograph at higher magnification of selected region in (a) and (d) micrograph at higher magnification at selected region in (b).	106
Fig. 5.4	Optical micrographs of heat-treated samples: (a) additive sample in 0° orientation showing very fine lath martensite (b) conventional sample showing coarser lath martensite	107
Fig. 5.5	Variation of wear rate as a function of applied load in specimens: (a) conventional as received (CM) and additive samples as-built (AB) in 0° , 45° and 90° orientations and (b) conventional heat treated (CM-HT) and additive manufactured in 0° , 45° and 90° orientations followed by heat treated (HT) conditions.	108

Fig. 5.6	Coefficient of friction (COF) vs load plots: (a) conventional as received (CM) and additive manufactured as-built (AB) in 0°, 45° and 90° orientations and (b) conventional heat treated (CM-HT) and additive manufactured in 0°, 45° and 90° orientations followed by heat treated (HT) conditions.	109
Fig. 5.7	Variation of coefficient of friction with time at 80 N load: (a) as built (AB) and Conventional as received (CM) specimen, (b) conventional heat treated (CM-HT) and additive manufactured followed by heat treated (HT) specimen.	110
Fig. 5.8	Erosion rate of additive and conventional samples in as built/as-received and heat-treated conditions.	111
Fig. 5.9	Worn surfaces of as received conventional sample (CM) and as-built additive samples (AB) in different orientations at 20N load: (a) CM (b) 0° AB (c) 45° AB and (d) 90° AB and their corresponding 3D profile images (a', b', c' and d').	112
Fig. 5.10	Worn surfaces of as received conventional sample (CM) and as-built additive samples (AB) in different orientations at 80 N load: (a) CM (b) 0° AB (c) 45° AB and (d) 90° AB and their corresponding 3D profile images (a', b', c' and d').	113
Fig. 5.11	Worn surfaces of heat-treated conventional and additive samples in different orientations: (a) CM-HT (b) 0° HT (c) 45° HT (d) 90° HT and their corresponding 3D profile images (a', b', c' and d').	114
Fig. 5.12	Eroded surfaces of as-built (AB) additive samples in different orientations and conventional as received (CM) sample: (a) 0° AB (b) 45° AB (c) 90° AB and (d) CM	115
Fig. 5.13	Eroded surfaces of heat-treated additive samples in different variations and conventional sample: (a) 0° HT (b) 45° HT (c) 90° HT and (d) CM-HT	116
Fig. 5.14	(a) SEM micrograph of eroded surface (b) cellular and columnar microstructure in the as-built samples (c) cross-sectional view of eroded sample and (d) high magnification image of (c).	117
Fig. 5.15	Schematic diagram depicting mechanisms of wear in M300 maraging steel: (a) abrasive wear at 20 N load and (b) adhesive wear at 80 N.	122
Fig. 5.16	Erosion mechanism of both AM and conventional samples in as received and heat-treated conditions.	123

Fig. 6.1	Schematic representation of three plates printed in different orientations, depicting layers, along with the exposer side during corrosion, shown by arrows.	125
Fig. 6.2	Optical micrograph of maraging steel: (a) Coarse microstructure in CM condition and (b) lath martensite in CM-HT condition.	126
Fig. 6.3	Optical micrograph depicting: (a) laser tracks with fine cellular and columnar structure (a') interlayer rotation in 0° AB condition and (b) very fine martensite with no tracks residue after heat treatment in 0° HT condition.	127
Fig. 6.4	Optical micrographs depicting: (a) very fine microstructure, (a') inclined melt pool in 45° AB condition and (b) martensite with partial melt pool characteristic in 45° HT condition.	127
Fig. 6.5	Optical micrographs depicting: (a) semi-elliptical melt pool, (a') series of layers with melt pool in 90° AB condition and (b) fine martensite with partial melt pool characteristics in 90° HT condition.	128
Fig. 6.6	(a) Potentiodynamic polarization curves of CM and AB condition in different orientations (b) Potentiodynamic polarization curves in AM-HT and CM-HT conditions.	129
Fig. 6.7	Nyquist plots in the CM and AB conditions.	131
Fig. 6.8	Nyquist plots in CM-HT and AM-HT conditions.	131
Fig. 6.9	Bode plot of CM and AB specimens in different orientations: (a) log-log plot of $ Z $ vs. log freq. (b) plot of phase angle vs. log freq.	132
Fig. 6.10	Bode plots of CM-HT and AM-HT specimens: (a) log-log plot of $ Z $ vs. log freq. (b) plot of phase angle vs. log freq.	132
Fig. 6.11	Equivalent circuit diagram of fitting EIS data. In this diagram R1, R2 and R3 represent the solution resistance, charge transfer resistance of outer region of passive film, and inner layer charge transfer resistance. QPE1, L1 is constant phase angle element of outer layer and inductance of inner layer respectively.	133
Fig. 6.12	XPS survey of maraging steel in different conditions, showing the presence of Fe, O, Ni, Mo, Ti, Co elements in the corrosion product.	136
Fig. 6.13	XPS peak spectra in 90° AB condition showing: (a) Oxygen O _{1s} peak spectra (b) Co _{2p} peak spectra (c) Ni _{2p} peak spectra.	138

Fig. 6.14	XPS peak deconvolution in CM samples: (a) Fe _{2p} peak spectra fitting showing iron hydroxide and oxide as a corrosion product (b) Mo _{3d} peak spectra fitting (c) Ti _{2p} XPS peak spectra.	138
Fig. 6.15	XPS peak fitting of 90°AB condition: (a) Fe _{2p} peak spectra fitting (b) Mo _{3d} spectra fitting (c) Ti _{2p} XPS peak spectra fitting.	139
Fig. 6.16	XPS peak fitting in CM-HT condition: (a) Fe _{2p} peak spectra (b) Mo _{3d} spectra fitting and (c) Ti _{2p} XPS peak spectra with negligible intensity.	139
Fig. 6.17	XPS peak spectra fitting of 45° HT sample for (a) Fe _{2p} peak (b) Mo _{3d} spectra (c) Ti _{2p} peak fitting which showed negligible intensity count.	140
Fig. 6.18	Corrosion surface morphology on CM specimen showing (a) uniform corrosion product on the surface (b) magnified view of corrosion product and passive layers with cracks and (c) EDS area scan of corrosion product.	142
Fig. 6.19	Corrosion surface morphology of 0° AB specimen showing (a) non uniform corrosion product on surface (b) magnified view of corrosion product (c) EDS area scan of corrosion product and (d) microstructural morphology of AB sample through passive layer.	143
Fig. 6.20	Corrosion surface morphology of 0° HT specimen showing: (a) non-uniform corrosion product on surface (b) magnified view of corrosion product and passive layer film crack (c) EDS scan of corrosion product.	144
Fig. 6.21	Side surface morphology of corroded specimens in different conditions showing: (a) very thin corroded film in CM samples (b) pitting along layer junction in 45° AB and (c) inter layer pitting corrosion in 90° AB.	145
Fig. 6.22	Side surface morphology of corroded specimen in different conditions: (a) CM-HT. (b) 45° HT and (c) 90° HT specimen.	146
Fig. 6.23	Mechanism of corrosion in the present maraging steel in as-built (AB) condition.	149
Fig. 6.24	Mechanism of corrosion in the present maraging steel in as-built (AB) and heat treated (HT) condition.	149

LIST OF TABLES

Table No.	Table Caption	Page No.
Table 1.1	Nominal chemical composition of maraging steels in wt%	16
Table 1.2	Mechanical properties of grade 300MS produced through Selective Laser Melting (SLM) and the conventional wrought route	25
Table 1.3	Summary of LCF results at varied strain amplitudes.	31
Table 2.1	Chemical composition of maraging steel (M300) used in the present work.	50
Table 2.2	Designation of different samples used for testing.	53
Table 3.1	Variation of surface roughness and density of as-built AM (additive manufactured) samples in different orientations.	65
Table 3.2	Volume fraction of phases in AM and AM-HT samples in different orientations.	72
Table 4.1	Values of residual stress in AB and HT samples.	80
Table 4.2	Tensile properties of AM and CM specimens of M300 steel in different conditions tested at a strain rate of 10^{-3} s^{-1} .	83
Table 4.3	Strength anisotropy (A_{IP}) and elongation anisotropic index (δ) of additive manufactured (AM) as built and heat-treated (HT) samples.	84
Table 4.4	Fatigue Life of M300 maraging steel in AM and CM conditions.	89
Table 5.1	Wear rates observed in conventional and additive samples in as-built and heat-treated conditions.	109
Table 5.2	Coefficient of friction for conventional and additive samples in as-built and heat-treated conditions.	110
Table 6.1	Electrochemical parameters of maraging steel in different conditions, extracted from polarization plots fitted in the Tafel region.	130
Table 6.2	EIS Data, simulation using CS Studio software for maraging steel in different conditions.	135
Table 6.3	Chemical composition of the passive film formed on maraging steel in different conditions, in aqueous solution of 3.5% NaCl, as determined from the XPS survey spectra.	137

Table 6.4 XPS peak fitting parameters were obtained for the reconstruction of spectra. 141

LIST OF SYMBOLS

Symbols and Abbreviations	Description
P	Laser Power
V	Scan Speed
T	Layer Thickness
D	Hatch spacing
P	Relative Density
R _a	Average surface roughness
R _q	Root mean square roughness
R _z	Average max. hight roughness
<i>P_{ct.El}</i>	Percentage Elongation
σ_{ys}	Yield Strength
σ_{UTS}	Ultimate tensile strength
e_f	Elongation upto fracture
e_u	Uniform elongation
A _{IP}	Strength anisotropy index
Δ	Elongation anisotropic index
σ_c	Cyclic compressive strength
σ_t	Cyclic Tensile strength
R	Stress Ratio
$\dot{\epsilon}$	Strain rate
$\Delta\epsilon/2$	Strain amplitude

$\Delta\varepsilon_e/2$	Elastic strain
$\Delta\varepsilon_p/2$	Plastic strain
$\Delta\sigma/2$	Stress amplitude
N_i	No. of cycle for crack initiation
N_f	No. of cycle to fatigue fracture
μ	Micro meter
Γ	Impedence constant
W	Angular frequency
Z	Impedence
F	Frequency

PREFACE

Additive manufacturing (AM), commonly known as 3D printing, is an industrial computer-controlled process that produces three-dimensional objects by depositing materials in layers on the base material. Additive manufacturing uses various materials depending on the printing process. These materials range from metal and alloys, thermoset polymers, thermoplastics, and ceramics to composites. In AM, production from prototypes to end-use parts can be done and processing is faster, cheaper, easier to use and more accessible compared to subtractive manufacturing methods, which are more complicated and expensive. Now-a-days, industries are adopting AM technology because it can greatly improve efficiency and agility while minimizing supply chain risk, while automated processes in AM can reduce the need for specialized labour. The latest industrial revolution, Industry 4.0, is encouraging the integration of intelligent production systems and advanced information technologies. Additive manufacturing (AM) is considered to be an essential process in this industrial revolution. There are two important techniques in metal additive manufacturing i.e., Powder Bed Fusion (PBF) and Direct Energy Deposition (DED). In powder bed fusion, required thickness of powder is spread on the base plate and the powder is fused selectively by laser or electron beam by computer-controlled software. In directed energy deposition, both metal powder and laser beam are guided through nozzle and the nozzle can move in X, Y and Z directions to achieve the given dimensions of parts layer by layer. Products manufactured by powder bed fusion are comparatively better in density and properties and hence powder bed fusion is preferred and the most adopted technique out of the industrially accepted technologies available. Practically, AM processed parts consist of stacking of series of laser scanned layers to get desired cross section and height. Due to complex heating and

cooling cycles and layer wise processing characteristics, microstructural inhomogeneities and non-uniform distribution of defects can occur which affect the properties of the as-built parts. The products may also have variation in properties in different build directions depending on the angle between layer orientation and application of load as well as exposure to different media. Hence it is necessary to investigate the effect of build orientation on behaviour of materials subjected to different kinds of loading and exposed to various environments.

The growth of any new technology is only possible if the product formed by the technology is reliable and efficient. The performance of AM parts with respect to build orientation need to be understood before placing them in a given application and the parts should function reliably and efficiently in different orientations. Also, the effectiveness of post-processing techniques such as heat treatment to reduce layered anisotropy and get enhancement in the performance of parts is required to be explored.

Maraging steel is an advanced high strength steel, specially used in many industries due to its unique properties. It is a high-strength, high-toughness and corrosion-resistant steel that is ideal for applications that require high-performance parts and can be strengthened through heat treatment, particularly ageing. Maraging steel is often used in applications that require high strength and toughness, such as aerospace and defence industries. It exhibits good weldability, machinability and corrosion resistance also which makes it an attractive option for use in many other industries such as oil and gas, medical and automotive sectors. Important reason for the adoption of maraging steel in additive manufacturing is its unique combination of properties such as high strength, high toughness, good weldability, corrosion resistance and age-hardening ability, which make it well-suited for producing high-performance parts with complex geometries. These excellent properties, combined with the growing popularity of additive manufacturing,

make maraging steel an attractive material for processing by AM which can find applications in various strategic sectors.

In view of this, maraging steel powder of 15-45 μm size was selected to build the samples in 0°, 45° and 90° build orientations. Further, the test coupons for tensile, fatigue, wear, erosion and corrosion behaviour were prepared and tested to investigate the effect of build orientation on various properties. The results obtained can be utilized for the improvement in design, quality and reliability of parts as per the applicability and usage of the product in intended functions.

OUTLINE OF THE THESIS

The thesis is organised into seven chapters as mentioned below.

Chapter 1 provides a comprehensive background on additive manufacturing and its classification, focusing specifically on powder bed fusion (PBF) / selective laser melting (SLM). The possibility of defects in SLM parts, such as lack of fusion, porosity and inconsistent material properties, are also discussed. The need for processing steels using additive manufacturing and the reasons for favouring maraging steel in AM, are mentioned. A literature review of the microstructure, tensile, low cycle fatigue, wear, erosion and corrosion behaviour of additively manufactured maraging steel is presented and it is found that there are very few studies that have investigated all of these properties comprehensively. Therefore, this work aims to fill this research gap and investigate the microstructure, tensile, low cycle fatigue, wear, erosion and corrosion behaviour of additively manufactured maraging steel in more detail. The chapter also discusses the effect of heat treatment on functionality of parts. With the help of literature, the process parameters were optimized by Ansys Additive software and also optimum heat treatment

was chosen which can enhance both strength and ductility. The motivation for the present research work is explained at the end of this chapter.

Chapter 2 presents a detailed description of the raw materials, processing techniques and experimental procedures employed in the course of the investigation. Divided into three sections, the first section focuses on the materials selection and processing techniques, including the parameters used for processing and the heat treatment given to the samples. The second section deals with the characterization of processed parts and different experimental and testing procedures for the samples. This includes the microstructural characterization of additively manufactured and conventional samples, along with the details of the geometry of tensile, wear, erosion and corrosion samples, testing procedures and parameters. The third section gives procedures adopted for the fractography of tensile and fatigue tested samples by SEM, as well as the analysis of worn, eroded and corroded samples by SEM, EDS and XPS.

Chapter 3 focuses on the investigation of the effect of build orientation on the microstructure and physical properties of maraging steel processed by Additive Manufacturing (AM) and conventionally manufactured (CM). The samples were processed in orientations of 0°, 45°, and 90° using Powder Bed Fusion using Laser Beam (PBF-LB) and were given solution treatment and aging. The density, surface roughness and microstructural characterization of all the samples were investigated and compared with those of CM samples. The presence of Ni₃Ti and Fe₂Mo precipitates after both AM processing and heat treatment was confirmed using Transmission Electron Microscopy (TEM). This study provides valuable insights into the influence of build orientation on the microstructure and physical properties of maraging steel, which can aid in the development of optimized processing parameters for AM.

Chapter 4 investigates the effect of build orientation on the mechanical behaviour of additive manufactured maraging steel compared to the behaviour of conventionally manufactured maraging steel. Tensile testing shows that the 45° orientation specimen exhibits the best combination of strength and ductility and heat treatment improves the tensile properties, reduces anisotropy and residual stresses. The sample built in 0° orientation exhibits longest fatigue life before heat treatment. Post-heat treatment is found to be necessary to improve fatigue behaviour further and unmelted regions resulting from processing are found to be the most detrimental and cause reduction in fatigue life. SEM analysis shows that cracks initiated from surface and inner defects. Overall, this chapter provides valuable inputs of the effects of build orientation on the mechanical behavior of additive manufactured maraging steel samples and the effect of post heat treatment.

Chapter 5 explores the wear and erosion behaviour of additively manufactured (AM) maraging steel in comparison with conventional materials. The study compares the wear and erosion characteristics of maraging steel with three different build orientations (0°, 45°, and 90°) with those of cast and hot-rolled samples. The wear and erosion behaviour of the as-built and heat-treated maraging steel samples were examined under various loads and the samples were analyzed using scanning electron microscopy (SEM) and atomic force microscopy (AFM). The results show that the wear rate increases with an increase in load and is influenced by build orientation, with 90° oriented samples exhibiting higher wear resistance in both as-built and heat-treated conditions. The erosion resistance of the conventional samples is inferior to that of the additive samples prior to heat treatment. However, after heat treatment, erosion resistance increases, and the erosion resistance of the 0° samples is found to be higher than those of the other build

orientations. The study provides insights into the potential of AM technology to produce wear-resistant components, with the 90° orientation found to be more wear-resistant, and heat treatment can further improve the wear and erosion resistance of the samples. The results of this study can assist in the selection of appropriate build orientation and heat treatment parameters for producing wear-resistant components using AM technology.

Chapter 6 describes the corrosion behaviour of additively manufactured (AM) maraging steel compared to the behaviour of conventionally produced maraging steel in a 3.5% NaCl solution. The study explores the impact of build orientation and solution and aging treatment on the corrosion resistance of the samples. The results show that as-built samples have increased resistance to corrosion with a decrease in the angle of inclination, as a result of structural heterogeneity and higher grain boundary density. However, heat treatment causes a decrease in corrosion resistance due to the precipitation of intermetallic phases and reverted austenite formation and the corrosion-resistant oxide layer is not observed on the heat-treated samples. The findings reveal a notable difference in pitting corrosion between the as-built and heat-treated samples, emphasizing the importance of optimizing build orientation and heat treatment parameters to enhance the corrosion resistance of AM maraging steel. These findings provide valuable information about the corrosion behaviour of AM maraging steel and suggest the need for further research to fully understand the relationship between microstructure, build orientation, and corrosion behaviour.

Chapter 7 summarizes the major conclusions of the thesis and suggests future research directions in the field of AM metals and alloys.